J Polym Res (2008) 15:205–212
DOI 10.1007/s10965-007-9160-4

Natural inorganic nanotubes reinforced epoxy resin nanocomposites

Mingxian Liu · Baochun Guo · Mingliang Du · Yanda Lei · Demin Jia

Received: 6 August 2007 / Accepted: 1 October 2007 / Published online: 17 November 2007

Abstract Natural occurred nanotubes, halloysite nanotubes, were modified by silane and incorporated into epoxy resin to form nanocomposites. The morphology of the nanocomposites was characterized by transmission electron microscopy (TEM). Dynamic mechanical analysis (DMA) and thermogravimetric analysis (TGA) were performed on the nanocomposites. Flexural property and coefficient of thermal expansion (CTE) of the nanocomposites were also determined. Comparing with the neat resin, about 40% increase in storage modulus at glassy state and 133% at rubbery state were achieved by incorporating 12 wt% modified HNTs into the epoxy matrix. In addition, the nanocomposites exhibited improved flexural strength, char yield and dimensional stability. TEM examination revealed a uniform dispersion of the nanotubes in the epoxy resin. The remarkably positive effects of the HNTs on the performance of the epoxy resin were correlated with the unique characteristics of the HNTs, the uniform dispersion and the possible interfacial reactions between the modified HNTs and the matrix.

Keywords Halloysite · Nanotube · Epoxy resin · Composite · Mechanical property

Introduction

Carbon nanotubes (CNTs) filled polymer nanocomposites have received much attention due to their interesting properties such as thermal and mechanical properties in recent years [1, 2]. The enhanced performances of the polymer composites were often explained by the characteristics of the nanotubes as the particle size and shape of fillers are important factors in determining the properties of the filled polymer composites [3]. A carbon nanotube is a hexagonal network of carbon atoms rolled up into a seamless, hollow cylinder, with each end capped with half of a fullerene molecule. Although similar in chemical composition to graphite, CNTs are highly isotropic and with a high aspect ratio, and it is this topology that distinguishes nanotubes from other carbon structures and gives them their unique properties. The unique nanostructure and properties of nanotubes are critical for the good mechanical properties of the obtained composites [4, 5]. Significant reinforcing effect for polymer matrix through incorporation CNTs has been reported. For example, a loading of 1 wt% MWNTs in PMMA exhibited increase in tensile toughness with a 170% improvement over pure PMMA [6]. Cadek *et al.* found that adding 1 wt% multi-walled CNTs to polyvinyl alcohol (PVA) increased the modulus and hardness by 1.8 times and 1.6 times, respectively [7]. Incorporation of 1 wt% CNTs to epoxy resin can lead to the 100% increased in Young's modulus, and meanwhile the tensile strength of the epoxy resin increased from 30 MPa to 41 MPa [8]. Chemical functionalization and alignment of CNTs can promote good dispersion, interfacial interaction and orientation of CNTs in polymer/CNTs composites, which play a dominant role in further development of the reinforcing effect of CNTs for polymer [9, 10]. However, the chemical functionalization process or alignment using external field of CNTs is relatively difficult to control. Furthermore, up to now, carbon nanotubes and some inorganic nanotubes reported were all artificial materials and the processes for their preparation are generally time-consuming and costly [11, 12]. These drawbacks of the synthesized nanotubes inhabit their industrial applications [2]. Therefore, exploring low cost and easily available nanotubes for the modifications of polymers are practically important.

M. Liu · B. Guo (✉) · M. Du · Y. Lei · D. Jia
Department of Polymer Materials and Engineering,
South China University of Technology,
Guangzhou 510640, China
e-mail: psbcguo@scut.edu.cn

Halloysite nanotubes (HNTs) are a kind of naturally deposited aluminosilicate with a high aspect ratio [13]. HNTs are inorganic rigid nanotubes and are reported as an effective modifier for polymers. Incorporating HNTs to polypropylene (PP) leads to higher flexural modulus and thermal stability of the polymer [14, 15]. Surface modification of inorganic fillers was a common and effective method for promoting the dispersion of fillers in polymer composites and led to further increased mechanical properties of the composites [16–19]. Many literatures reported the methods for chemical functionalized of CNTs and the effects of modification on the performance of the composites [20–24]. For instance, acid modified CNTs can be dispersed more uniformly than unmodified CNTs in polyimide matrix. Consequently, the tensile strength and modulus of the modified CNTs filled polyimide were 13.7% and 15.6% higher than those for the control sample [25]. Surface modification of HNTs can also enhance the dispersion of HNTs in the polymer matrix and consequently enhance the mechanical and thermal properties of the nanocomposites [26]. Comparing with CNTs and the synthesized inorganic nanotubes such as silica nanotubes [27] and titania nanotubes, the naturally occurred HNTs is much cheaper. In addition, unlike CNTs, HNTs are inherently insulating. Thus, composite materials fabricated by dispersing HNTs in an insulating polymer have good mechanical properties without sacrifice of insulating properties of the polymer. Like other inorganic nanotubes, HNTs have much lower aspect ratio compared with CNTs. Furthermore, compared with other synthesized inorganic nanotubes, precision control of the length and diameter of HNTs is impossible as they are formed naturally. Chemically, the surface properties of HNTs are predominantly those of aluminols. While the surface chemistries of silica nanotubes, titania nanotubes and CNTs are determined by silanols, titanols and defects of the hexagonal network of carbon atoms, respectively. In summary, HNTs are interesting candidate for preparing the polymer nanocomposites with unique structure and performance.

In the present work, silane bearing glycidyl group treated HNTs were incorporated to a cyanate ester cured epoxy resin. The effect of the HNTs on the mechanical properties, thermal stability and dimensional stability of the epoxy resin were investigated. The variation in the properties of the nanocomposites was correlated with the microstructure of the nanocomposites, which were examined by TEM.

Experimental

Raw materials

The epoxy resin used was a liguid diglycidyl ether of bisphenol A (GELR-128, epoxy equivalent of 184–190 g/eq, Grace T. H. W., Taiwan). The hardener, bisphenol A dicyanate ester (AroCy B-10) was purchased from Ciba Specialty Chemical Corp. Cyanate ester was selected as the hardener as it can co-cure with epoxy resin. The HNTs, were mined from Shennongjia, Hubei, China. The elemental composition of HNTs by X-ray fluorescence (XRF) was determined as follows (wt%): SiO_2, 58.91; Al_2O_3, 40.41; Fe_2O_3, 0.275; TiO_2, 0.071. The Brunauer–Emmett–Teller (BET) surface area of purified HNTs is approximately 54.45 m^2/g. Coupling agent γ-glycidoxypropyltrimethoxy silane (Z-6040) was supplied by Dow Corning Co., Ltd. The chemical structures of the epoxy resin, the hardener and the silane are represented as follows:

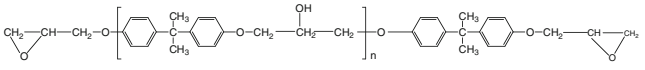

epoxy resin

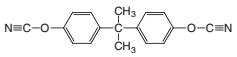

cyanate ester

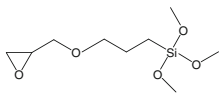

silane

Purification and modification of HNTs

Raw halloysite was purified as the method introduced in the reference [28]. Typical procedure is described below. A 10 wt% water solution of halloysite was prepared by slow addition water to dry halloysite. Then 0.05 wt% sodium hexametaphophate was added in the solution while stirring. The solution was stirred for 30 min and standing for 20 min under room temperature. The clay aggregate and impurities was precipitated in the bottom and were removed by filtration. The upper solution was carefully collected and the resulting HNTs was separated by centrifugation and dried at 80°C in air for 5 h.

The silylation of HNTs was performed according to the below procedure. (1) To a 250-mL Erlenmeyer flask halloysite (10 g) and an ethanol/water mixture (50/50 vol/vol, 100 mL) were added. The mixture was stirred until the clay dispersed. (2) The pH value was adjusted to about 5 with acetic acid. (3) In a separate beaker the silane (2.3 g) was added to an ethanol/water solution (50/50 vol/vol, 10 mL). (4) This solution was added to the clay dispersion and stirred for 2 d. (5) The HNTs were collected on a Buchner funnel and redispersed by stirring in methanol (100 mL) for 2 h, collected again, and stirred again in methanol (100 mL) for 2 h. The modified HNTs were collected on a Buchner funnel and dried at 80°C for 6 h. The modified HNTs are abbreviated as m-HNTs.

Characterization of m-HNTs

Thermogravimetric analysis of the purified pristine HNTs and m-HNTs were conducted under nitrogen atmosphere with NETZSCH TG209F1 at a heating rate of 10°C/min from 30°C to 800°C. Pore analysis of the purified HNTs and m-HNTs were investigated using nitrogen adsorption-desorption isotherms with Micromeretics ASAP 2020 analyzer. The pore-size distributions were computed by applying the Barrett–Joyner–Halenda (BJH) methods.

Preparation of nanocomposites

The m-HNTs were dispersed in epoxy resin at 70°C under stirring for 60 min and then degassed. The hardener was added and stirred for 10 min to ensure the good mixing of the component. The resulting mixture was degassed for 30 min and poured into steel molds with Teflon coating. The weight ratio of epoxy resin/hardener was 100/40. The samples were cured according to the curing schedule of 150°C/2h+180°C/1h+200°C/2h. The samples were cooled to room temperature over 8 h. The HNTs content in epoxy/HNTs composites varied from 4 to 12 wt%.

Characterization of the nanocomposites

Transmission Electron Microscopy (TEM): Ultrathin sections (200 nm) of the samples were cut using an unltramicrotome (EM ULTRACUT UC, Leica) and the sections were supported by holey carbon film on Cu-grids. TEM analysis of the nanocomposites was carried out with Philips Tecnai 12 transmission electron microscopy.

- Dynamic Mechanical Analysis (DMA): Dynamic mechanical analysis was conducted with a NETZSCH Instruments DMA 242 at an oscillation frequency and heating rate of 1.0 Hz and 5°C/min respectively. The 3-point bending mode was selected and the experiments were conducted under nitrogen purging.
- Flexural Test: Flexural properties of the nanocomposites were determined using an Instron 4465 Universal tester according to ASTM D90. Tests were conducted at room temperature with a cross-head speed of 2 mm·min^{-1} and at least 4 specimens per composition were tested.
- Coefficient of Thermal Expansion (CTE): CTE of the samples was measured with a NETZSCH DIL 402 PC at a heating rate of 10°C/min from room temperature to 160°C.
- Thermogravimetric Analysis (TGA): TGA of the nanocomposites was carried out under N_2 atmosphere with NETZSCH TG209F1 at a heating rate of 10°C/min from 30°C to 800°C.

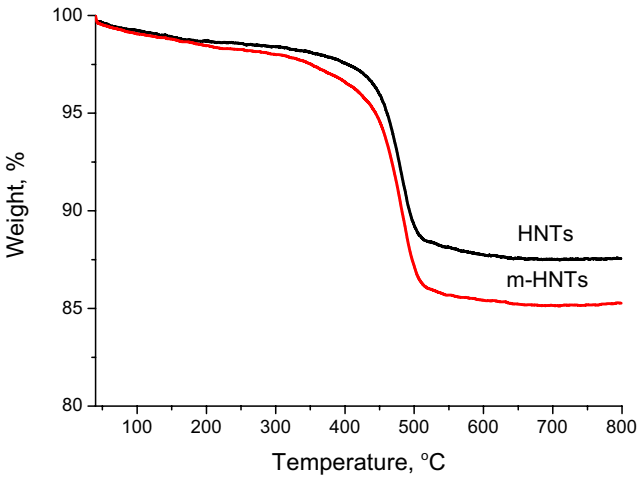

Fig. 1 TGA curves of HNTs and m-HNTs

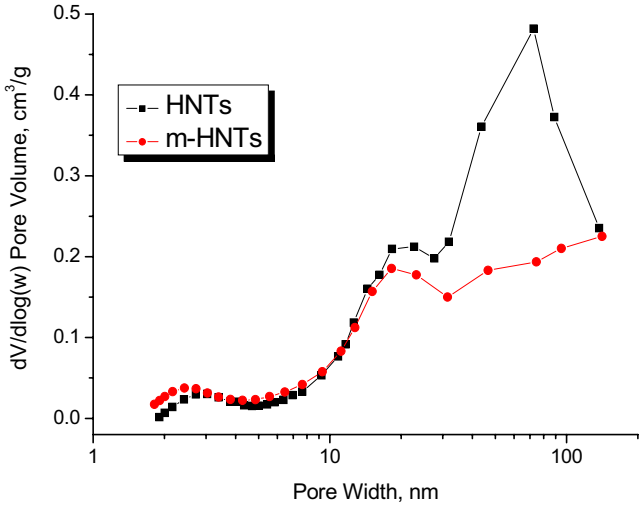

Fig. 2 Pore distributions of HNTs and m-HNTs

Results and discussion

Characterization of HNTs and m-HNTs

HNTs are hydrophilic and typically agglomerated in the as-received condition. HNTs were firstly purified to remove any impurities, such as quartz and illite etc. The purified HNTs were then treated by silane to facilitate the dispersion of the nanotubes in hydrophobic epoxy matrix. The silane was successfully grafted on the HNTs as indicated by the results of TGA and pore analysis. The weight loss curves for the HNTs before and after the modification are presented in Fig. 1. As shown, the weight loss of m-HNTs is increased compared with that of the HNTs. The increased weight loss may be due to the decomposition of the grafted

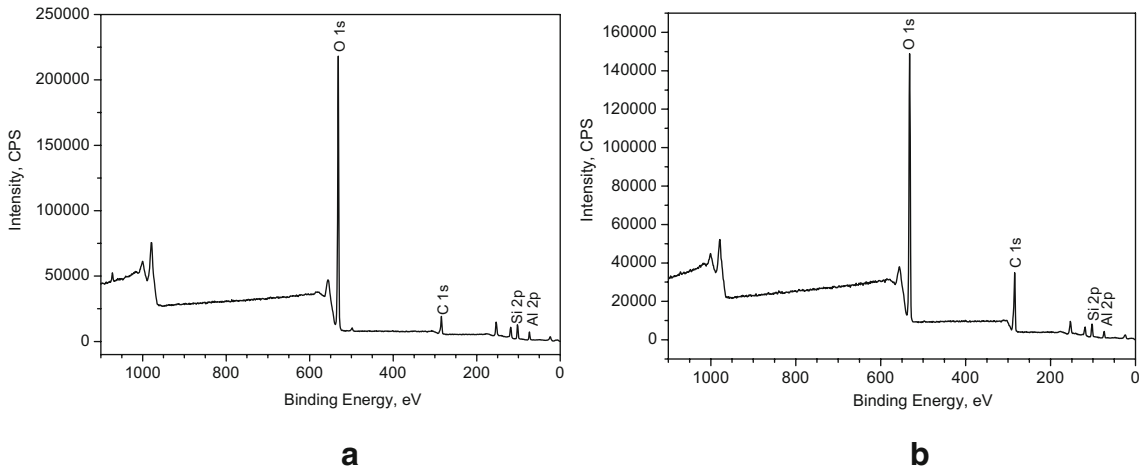

Fig. 3 Low-resolution XPS survey of the HNTs (**a**) and m-HNTs (**b**)

organic molecules on the HNTs surface. The graft weight is calculated as 2.4 wt% relative to the weight of HNTs. As the graft weight is relatively low, the verification of the graft by the comparison of FTIR spectra was unsuccessful. Pore size and distribution analysis of nanoparticles measured by nitrogen adsorption and calculated by BJH method is an effective method for detecting the surface microstructure variation [29]. Figure 2 shows the pore size distributions of the purified HNTs and m-HNTs. The mesopores and macropores coexist on the HNTs, on which the peaks around 20 and 50 nm are attributed to the lumens of the nanotubes and pores among the tubes respectively. The peak for the pore of 50 nm almost disappears after the silylation of HNTs. This may be related with the change of the surface properties of HNTs after modification. Since HNTs is tubular with high aspect ratio, wrapping with organic molecules on the HNTs surface may results in less agglomeration, leading to reduced larger pore formed by lap jointing of the tubes.

To further confirm the successful grafting of the silane onto the HNTs surface, XPS was performed to examine the surface chemical composition of HNTs and m-HNTs. The low-resolution XPS survey spectra of the HNTs and m-HNTs are shown in Fig. 3. The characteristic elements of HNTs, including oxygen, silicon and aluminum, were detected. The C 1s peak of carbon element observed in the Fig. 3 (a) was attributed to the impurities of the HNTs. Table 1 summarizes the characteristic XPS data. It can be seen that the detected relative concentrations of silicon, aluminum of m-HNTs are substantially lower than those for HNTs. The oxygen relative concentration was also slightly decreased. In addition, the carbon concentration in the m-HNTs increases remarkably. These results can be explained by the effective wrap of silane on m-HNTs after treatment. As the sampling depth of XPS measurement is typical 3–5 nm, the abundant of the organic composition (typically the carbon) on the m-HNTs surface after modification was the origin of the increased relative concentrations of carbon and decreased relative concentrations of silicon and aluminum. Noticeably, after the treatment, the decrease in aluminum content (35.8 %) is more remarkable than that for silicon (28.7%). This may be attributed to the following two facts. First, the aluminum and silicon mainly located in the inner side and outside of HNTs respectively. As a consequence, more signals for silicon are detected. Second, the modification with silane introduces silicon atoms onto the surface of the HNTs. The above XPS result further verifies the successful modification of HNTs.

Table 1 XPS atomic content (at.%) for the HNTs and m-HNTs

Atom	HNTs	m-HNTs
C	15.30	38.17
O	54.33	41.14
Si	16.66	11.88
Al	13.72	8.81

Morphology of epoxy resin/m-HNTs nanocomposites

Generally, dispersion state of the fillers in polymer matrix is one of the critical factors in determining the mechanical properties of nanocomposites [3, 30]. Uniform dispersion of filler especially in nanoscale leads to high mechanical properties of composites. On the contrary, the aggregated fillers in the polymer matrix act as the stress-centralized points, leading to the deteriorated properties. Figure 4 shows the TEM photos of the nanocomposite. It can be seen that the HNTs are dispersed in the epoxy resin individually with relatively low HNTs loading, which may due to the compatibility between m-HNTs and epoxy resin.

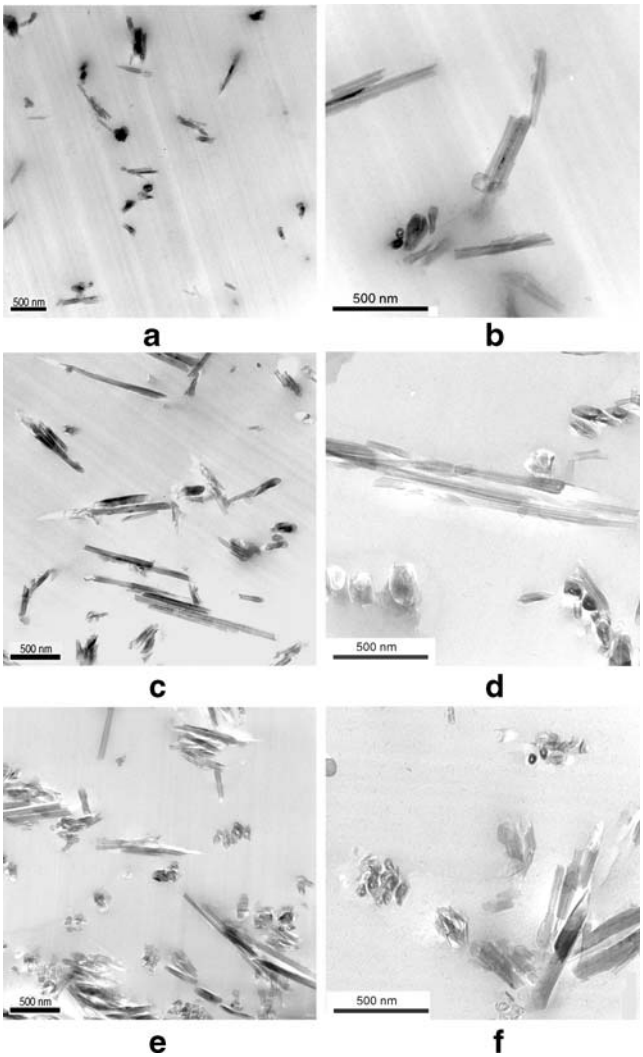

Fig. 4 TEM photos of the epoxy/m-HNTs nanocomposites. (**a**–**b**) 4 wt% m-HNTs; (**c**–**d**) 8 wt% m-HNTs; (**e**–**f**) 12 wt% m-HNTs. The black circles with *white core* in the photos represent the section of nanotubes cut by the knife in the sample preparation process before observation

The individually separated HNTs and aggregated HNTs coexist in the sample with relatively higher HNTs loading (12 wt%). The aggregation of HNTs may be the origin for the decreased flexural strength of the nanocomposites with relatively higher HNTs loading (12 wt%) as discussed in the below flexural test result.

Viscoelastic properties of epoxy resin/m-HNTs nanocomposites

The dynamic modulus versus temperature plots of the nanocomposites are shown in Fig. 5. Table 2 summarizes the value of storage modulus at glassy state and rubbery state of the nanocomposites. From Fig. 5 and Table 2, the storage modulus of the epoxy is significantly higher than the neat epoxy. About 40% increase in storage modulus at 50°C and 133% at 210°C was achieved in the composite incorporating 12 wt% m-HNTs. The significant increased mechanical properties of the nanocomposites were attributed to the unique nanostructure and property of the HNTs since HNTs are rigid silicate nanotubes with high strength and stiffness. The theoretical strength and modulus of alumina silicate are as high as 26 GPa and 120 GPa, respectively [31]. In addition, the good compatibility between m-HNTs and the epoxy matrix may also play an important role in the reinforcing effect. The treatment of HNTs by silane makes the surface of HNTs organophilic and reactive towards the resin system. Consequently, the m-HNTs are compatible with the matrix and could chemically be linked with the matrix after curing. When the load was applied on the nanocomposites, the good interfacial bonding makes the load effectively transferred from the matrix to the rigid inorganic phase. Therefore, the nanocomposites exhibit higher modulus even at the elevated temperatures. Synthesized inorganic nanotubes also show positive effect on the mechanical properties of polymer. Byrne *et al.* prepared polystyrene-TiO_2 nanotube composite films by a solution casting technique [32]. The composite films showed 18% increase in Young's modulus and up to 30% increase in tensile strength at extremely low nanotubes volume fractions of 10^{-4}. Figure 6 shows the tan δ versus temperature plots of the nanocomposites. It is observed that the tan delta value at T_g of the nanocomposites decrease by the incorporation of m-HNTs, although the trend is not consistent. As the HNTs content increases from 2 and 4 wt.-%, the height of the loss peak decreases gradually. The decreased tan delta is due to the restricted mobility of the polymer chains by the uniformly dispersed rigid nanotubes

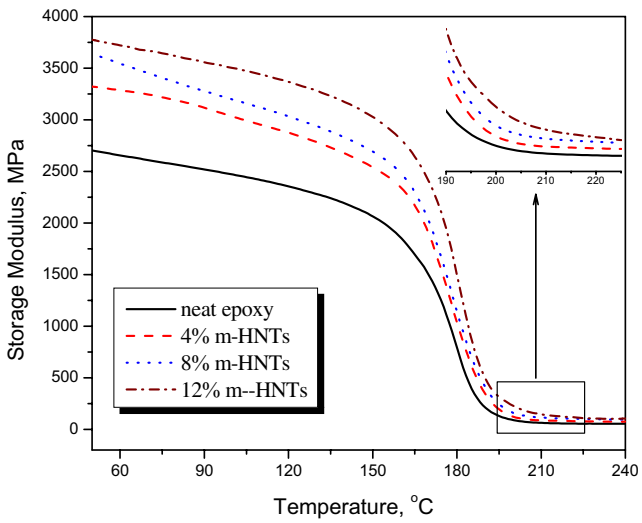

Fig. 5 Storage modulus versus temperature plots of the epoxy/m-HNTs nanocomposites

Table 2 Storage modulus and glass-transition temperature of epoxy/m-HNTs nanocomposites

Samples	E′ at 50°C (MPa)	Increase percentage (%)	E′ at 210°C (MPa)	Increase percentage (%)	T_g (°C)
Neat resin	2,701	–	62.8	–	189.2
4.0 wt% m-HNTs	3,321	23.0	87.4	39.2	189.1
8.0 wt% m-HNTs	3,637	34.7	114.9	83.0	188.1
12.0 wt% m-HNTs	3,775	39.8	146.2	132.8	193.1

[33]. However, overloading of the m-HNTs (12 wt%) increases the tan delta value at T_g, which may be attributed to the aggregation of m-HNTs at relatively higher content in the epoxy resin. Compared with that of the nanocomposites with uniformly dispersed nanotubes, the amount of confined polymer chains among the nanotubes was less in the nanocomposites with some aggregated m-HNTs. Therefore, the ability of aggregated m-HNTs for restricting the mobility of polymer chain decreases somewhat. The glass transition temperature values were also summarized in Table 2. It can be seen that addition of the m-HNTs did not significantly affect the measured glass transition temperature, and all values lay within the range 190±3°C. The results complement other findings for epoxy/nanoclay systems which report either modest decreased or little effect upon T_g of the nanoclay. [34–36] For examples, Zilg *et al.* [37] have found that effectively intercalated epoxy systems significantly decrease the T_gs of the final resin system. However, the increased glass transition temperatures of the nanoparticles filled epoxy systems were also widely reported [38–41]. The increased T_g was often attributed to the 'adsorbed layer' effect as the polymer chains being tied down by the surface of the silicate. In the present work, the chemical reaction during curing of the resin may be rather more complex due to the complicated chemical variation of the cyanate ester take place during heating. Hence it is much more difficult to identify precious origins for the slightly changed T_g.

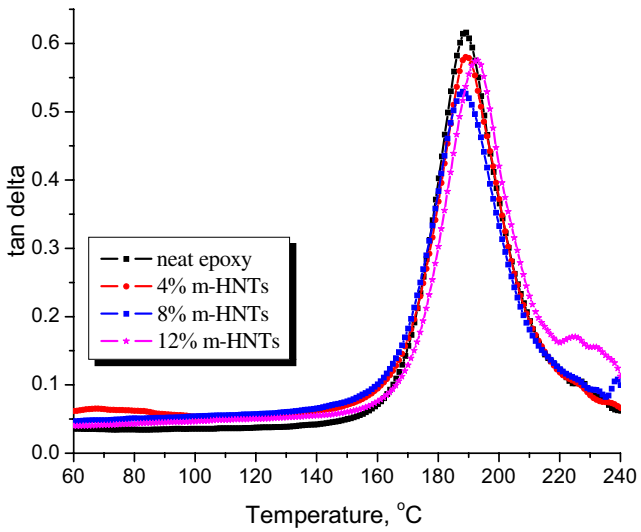

Fig. 6 Tan δ versus temperature plots of epoxy/m-HNTs nanocomposites

Flexural properties of epoxy resin/m-HNTs nanocomposites

It has been reported previously that incorporating the HNTs into polymer may effectively increase the flexural properties of the resulted polymer composites. The flexural modulus of the PP/HNTs nanocomposites with 30 phr HNTs, for instance, was 50% higher than that for the neat PP. PP composite with 30 phr HNTs modified by silane even showed 75% higher modulus than that for the neat PP [26]. The effects of HNTs on the flexural strength and flexural modulus of the epoxy resin were shown in Table 3. As shown, the flexural strength and flexural modulus of the composites increase gradually with HNTs content. The flexural modulus of the nanocomposites with 8 wt% m-HNTs is 18.2% higher than that of the neat epoxy. However, over loading HNTs (12 wt%) leads to decreased flexural strength and only minimal further increase in flexural modulus. This can be explained by the aggregation of m-HNTs in the epoxy matrix as shown in the above TEM photos. It is well known that particle aggregation are weak points in the materials and is the primary reason of reduced strength of materials even though the modulus is slightly increased [42].

CTE of epoxy resin/m-HNTs nanocomposites

The high dimensional stability (low CTE) of the epoxy resin is crucial to the fabrication of highly integrated printed circuit board [43, 44]. Lowering the CTE of epoxy

Table 3 Flexural modulus and flexural strength of epoxy/m-HNTs nanocomposites

Samples	Flexural Strength (MPa)	Flexural Modulus (GPa)
Neat resin	47	3.26
4.0 wt% m-HNTs	100	3.65
8.0 wt% m-HNTs	107	3.85
12.0 wt% m-HNTs	91	3.98

Table 4 CTE of the epoxy/m-HNTs nanocomposites at different temperature range

Samples	CTE 25–100°C	Decrease	CTE 100–160°C	Decrease
wt%	ppm/°C	%	ppm/°C	%
Neat resin	51.26	–	77.26	–
4.0	48.75	4.9	69.42	10.1
8.0	48.13	6.1	70.14	9.2
12.0	46.34	9.6	66.98	13.3

Table 5 Char yield of the epoxy/m-HNTs nanocomposites

Samples	Char yield at 800°C (%)	Calculated char yield at 800°C (%)
m-HNTs	85.27	–
neat epoxy	9.59	–
4.0 wt% HNTs	15.89	12.62
8.0 wt% HNTs	18.09	15.64
12.0 wt% HNTs	20.41	18.67

by inclusion of inorganic is a common and effective method [45, 46]. For example, because of the exceptionally low CTE of silica, which is only 0.5 ppm/°C, the silica filled composite materials have attracted much attention in reducing the CTE of polymer composites [47]. The CTE values of the composites are summarized in Table 4. It is shown that the CTE of the nanocomposites decreases with m-HNTs content. The tendency is more obviously at relatively high temperature. The CTE at higher temperature (100–160°C) for the composites with 12 wt% m-HNTs is determined as 66.98 ppm/°C, which is 13.3% lower than that of the neat epoxy resin. This may be attributed to the combinational effects of the high dimensional stability of HNTs, good dispersion of m-HNTs and the possible interfacial reaction between m-HNTs and the matrix.

TGA of epoxy resin/m-HNTs nanocomposites

TGA measurement was carried out to obtain information on the effect of HNTs on the thermal stability of the nanocomposites. Figure 7 shows the TGA curves of the epoxy/m-HNTs nanocomposites. It can be seen the thermal stability of the nanocomposites increases with HNTs at higher temperature (400~450°C), although almost little effect on the initial decomposition. The present result was good consistent with other earlier reported effects of silicate on the decomposition of epoxy resin nanocomposites [34, 48]. The degradation mechanism of an epoxy resin can be broadly understood in terms of a two-step process, starting with dehydration and followed by chain scission [49]. So HNTs can effectively depress the decomposition of the chain scission of the epoxy matrix, which is similar with the effect of HNTs in the polyvinyl alcohol nanocomposites [50]. The char yields at 800°C are summarized in Table 5. The char yield of the nanocomposites may theoretically be calculated according to the char yields of the neat epoxy resin and m-HNTs. The calculated char yields of the nanocomposites are also summarized in Table 5. Obviously, the char yields of the nanocomposites are higher than the calculated values. The increased the char yield of the epoxy resin may be attributed to the unique flame retardant effects of HNTs [15]. The result indicated that HNTs may increase the charring of the epoxy resin and consequently lead to somewhat enhanced flame retardancy of the resin.

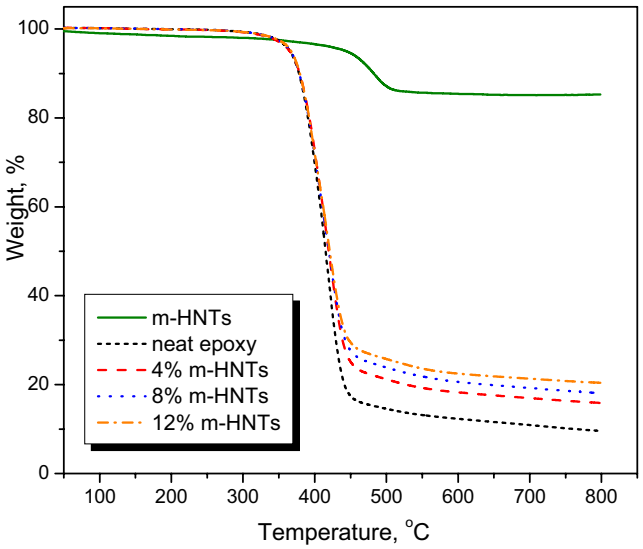

Fig. 7 TGA curves of epoxy/m-HNTs nanocomposites

Conclusions

Natural occurred nanotubes, halloysite nanotubes, were modified by silane and incorporated into epoxy resin to form nanocomposites. The modified HNTs could remarkably increase the storage moduli of the nanocomposites especially those at rubbery state. The nanocomposites exhibited improved flexural strength, char yield and dimensional stability. Individually dispersed HNTs were found in the composites with relatively low HNTs loading. The individually separated HNTs and aggregated HNTs coexisted in the sample with relatively higher HNTs loading. The remarkably positive effects of the HNTs on the performance of the epoxy resin were correlated with the unique characteristics of the HNTs, the uniform dispersion and the possible interfacial reactions between the modified HNTs and the matrix.

Acknowledgment This work was financially supported by the National Natural Science Foundation of China with grant number of 50603005.

References

1. Hussain F, Hojjati M, Okamoto M, Gorga RE (2006) J Compos Mater 40:1511–1575
2. Breuer O, Sundararaj U (2004) Polym Compos 25:630–645
3. Rothon RN (1999) Adv Polym Sci 139:67–107
4. Coleman JN, Khan U, Blau WJ, Gun'ko YK (2006) Carbon 44:1624–1652
5. Andrews R, Weisenberger MC (2004) Curr Opin Solid State Mater Sci 8:31–37
6. Gorga RE, Cohen RE (2004) J Polym Sci Part B: Polym Phys 42:2690–2702
7. Cadek M, Coleman JN, Barron V, Hedicke K, Blau WJ (2002) Appl Phys Lett 81:5123–5125
8. Bai J (2003) Carbon 41:1325–1328
9. Xie XL, Mai YW, Zhou XP (2005) Mater Sci Eng R 49:89–112
10. Moniruzzaman M, Winey KI (2006) Macromolecules 39:5194–5205
11. Wu XW, Ruan JF, Ohsuna T, Terasaki O, Che SN (2007) Chem Mater 19:1577–1583
12. Wu X, Jiang QZ, Ma ZF, Fu M, Shangguan WF (2005) Solid State Commun 136:513–517
13. Joussein E, Petit S, Churchman J, Theng B, Righi D, Delvaux B (2005) Clay Miner 40:383–426
14. Du ML, Guo BC, Liu MX, Jia DM (2007) Polym J 39:208–212
15. Du ML, Guo BC, Jia DM (2006) Eur Polym J 42:1362–1369
16. He FA, Zhang LM, Zhang F, Chen LS, Wu Q (2006) J Polym Res-Taiwan 13:483–493
17. Bauer F, Mehnert R (2005) J Polym Res-Taiwan 12:483–491
18. Liao CS, Ye WB (2003) J Polym Res-Taiwan 10:241–246
19. Chang CC, Wei KH, Chang YL, Chen WC (2003) J Polym Res-Taiwan 10:1–6
20. Khabashesku VN, Pulikkathara MX (2006) Mendeleev Commun 2:61–66
21. Wu HL, Wang CH, Ma CCM, Chiu YC, Chiang MT, Chiang CL (2007) Compos Sci Technol 67:1854–1860
22. Yuen SM, Ma CCM, Chiang CL, Lin YY, Teng CC (2007) J Polym Sci Part A: Polym Chem 45:3349–3358
23. Liu JQ, Xiao T, Liao K, Wu P (2007) Nanotechnology 18, Art. No. 165701
24. Yuen SM, Ma CCM, Wu HH, Kuan HC, Chen WJ, Liao SH, Hsu CW, Wu HL (2007) J Appl Polym Sci 103:1272–1278
25. Yuen SM, Ma CCM, Lin YY, Kuan HC (2007) Compos Sci Technol 67:2564–2573
26. Du ML (2007) Ph.D. Dissertation. South China University of Technology
27. Zhang YH, Li YQ, Li GT, Huang HT, Chan HLW, Daoud WA, Xin JH, Li LF (2007) Chem Mater 19:1939–1945
28. Shchukin DG, Sukhorukov GB, Price RR, Lvov YM (2005) Small 1:510–513
29. Miyata T, Endo A, Ohmori T, Akiya T, Nakaiwa M (2003) J Colloid Interface Sci 262:116–125
30. Meng XY, Wang Z, Tang T (2006) Mater Sci Technol 22:780–786
31. Mecholsky JJ Jr (2001) Fractography, fracture mechanics and fractal geometry: an integration. In: Varner JR, Frechette VD, Quinn GD (eds) Fractography of glasses and ceramics III, ceramic trans, vol 64, Am Ceram Soc
32. Byrne MT, McCarthy JE, Bent M, Blake R, Gun'ko YK, Horvath E, Konya Z, Kukovecz A, Kiricsi I, Coleman JN (2007) J Mater Chem 17:2351–2358
33. d'Almeida JRM, Monteiro SN, Menezes GW, Rodriguez RJS (2007) J Reinf Plast Compos 26:321–330
34. Dean K, Krstina J, Tian W, Varley RJ (2007) Macromol Mater Eng 292:415–427
35. Becker O, Varley R, Simon G (2002) Polymer 43:4365–4373
36. Brown JM, Curliss D, Vaia RA (2000) Chem Mater 12:3376–3384
37. Zilg C, Thomann R, Finter J, Mulhaupt R (2000) Macromol Mater Eng 280/281:41–46
38. Yung KC, Wang J, Yue TM (2006) Adv Compos Mater 15:371–384
39. Brown JM, Curliss D, Vaia RA (2000) Chem Mater 12:3376–3384
40. Basara G, Yilmazer U, Bayram G (2005) J Appl Polym Sci 98:1081–1086
41. Naous W, Yu XY, Zhang QX, Naito K, Kagawa Y (2006) J Polym Sci Part B: Polym Phys 44:1466–1473
42. Hussain F, Chen JH, Hojjati M (2007) Mater Sci Eng A 445:467–476
43. Imai T, Sawa F, Nakano T, Ozaki T, Shimizu T, Kozako M, Tanaka T (2006) IEEE T DIELECT EL IN 13:319–326
44. Yung KC, Wu J, Yue TM, Xie CS (2006) J Compos Mater 40:567–581
45. Yung KC, Wang J, Yue TM (2006) Adv Compos Mater 15:371–384
46. Koerner H, Hampton E, Dean D, Turgut Z, Drummy L, Mirau P, Vaia R (2005) Chem Mater 17:1990–1996
47. Sun YY, Zhang ZQ, Wong CP (2006) IEEE Trans Compon Packag Technol 29:190–197
48. Liu WC, Varley RJ, Simon GP (2007) Polymer 48:2345–2354
49. Bellenger V, Fontaine E, Fleishmann A, Saporito J, Verdu J (1984) J Polym Degrad Stab 9:195–208
50. Liu M, Guo B, Du M, Jia D (2007) Appl Phys A 88:391–395